ON THE ENERGY POTENTIAL OF DAYTIME RADIATIVE COOLING FOR URBAN HEAT ISLAND MITIGATION

Authors: Laura Carlosena 1,2,4*, ORCID 0000-0003-2068-8044; Álvaro Ruiz-Pardo, 3, ORCID 0000-0002-1321-1478; Jie Feng, 4; Olatz Irulegi, 1; Rufino J. Hernández Minguillón 1,2, ORCID 0000-0001-5322-9659; Mattheos Santamouris, 4, ORCID 0000-0001-6076-3526.

1 Architecture Department, University of the Basque Country UPV/EHU, 2 ah asociados, 3 Department of Thermal Machines and Engines, University of Cadiz, 4 Faculty of the Built-Environment, University of New South Wales

* Corresponding author lcarlosena001@ikasle.ehu.eus

Escuela Técnica Superior de Arquitectura

Plaza Oñati, 2

20018 Donostia - San Sebastián

KEYWORDS

Daytime radiative cooling; sensitivity analysis; spectrally selective materials; cooling potential; Urban Heat Island.

ABSTRACT

The objective of this paper is to present the potential of daytime radiative cooling materials as a strategy to mitigate the Urban Heat Island effect. To evaluate the cooling potential of daytime radiative cooling materials, 15 theoretical materials and seven existing materials were simulated: two radiative cooling materials, a coolmaterial, two white paints, a thermochromic paint and a construction material. The novelty of this study is that it shows that the optimal spectral characteristics of radiative cooling materials depending on the climate conditions and the type of application. A sensitivity analysis was performed to evaluate the impact of each wavelength emissivity on the ability to achieve sub-ambient radiative cooling. The sensitivity analysis comprised a total of 90 theoretical materials with 15 different wavelength combinations and 6 emissivity values. The heat transfer model, which includes conduction, convection, and radiation, was developed using a spectrally-selective sky model. Two conditions were considered: a very conductive surface and a highly insulated one. All the materials were simulated in two cities that suffer from the Urban Heat Island effect—Phoenix and Sydney. The mean surface temperature reduction achieved was 5.30 ºC in Phoenix and 4.21 ºC in Sydney. The results presented suggest that the type of application (active or passive) is a determinant factor in the design of radiative cooling materials. Modifying the spectra of the materials led to a substantial change in the cooling potential. A material that performs well in a dry climate as a passive solution could perform poorly as an active solution.

HIGHLIGHTS

- Daytime radiative cooling materials are studied in two cities with Urban Heat Island
- Contribution of wavelength band to the ability to achieve sub-ambient temperatures
- Materials studied under highly-insulated and highly-conductive conditions
- Material’s behavior strongly depends on the location and the type of application

Nomenclature	
c	Fraction of sky covered by clouds
E_b	Blackbody radiation W/m^2
G	Irradiance W/m^2
h	Convective heat transfer $W/(m^2K)$
I	Solar irradiation W/m^2
J	Radiosity W/m^2
q	Heat flux W/m^2
T	Temperature K
v	Wavenumber $1/m$
Greek letters	
ε	Emissivity
Subscripts	
cd	Conduction
cv	Convection
r	Radiation
s	Surface studied
sun	Solar
Δv	A wavenumber range or band

1. Introduction

Nowadays, half of the world’s population lives in urban areas (*World Urbanization Prospects*, 2014) and consumes 75% of the primary energy sources, emitting between 50 and 60% of greenhouse gases (“Energy – UN-Habitat,” n.d.). Furthermore, the world’s urban population is expected to increase by more than two-thirds by 2050, reaching 6.3 billion (*World Urbanization Prospects*, 2014), with nearly 90% of this rise taking place in cities across Asia and Africa. CO_2 emissions increase proportionately with population due to energy use (O'Neill et al., 2012). A 1% increase in the urban population is estimated to increase energy consumption by 2.2% (Santamouris et al., 2001). The global energy demand is predicted to increase by more than 25% if the IEA's New Policies Scenario (rising incomes and an extra 1.7 billion people) is followed (International Energy Agency, 2018).

Higher urban temperatures are due to the positive thermal balance of urban areas in comparison with rural areas, caused by (i) the significant release of anthropogenic heat, (ii) the excess storage of solar radiation by city structures, (iii) the lack of green spaces and cold sinks, (iv) the non-circulation of air in urban canyons, and (v) the reduced ability of emitted infrared radiation to escape into the atmosphere (Oke et al., 1991). This phenomenon, known as the Urban Heat Island (UHI), is well documented in more than 400 cities around the world (Santamouris, 2019), and the total number of reported cities is increasing rapidly. The average UHI varies between 0.5 ºC to 7 ºC, where 90% of the data is below 4.5 ºC (Santamouris, 2020). As ambient air temperature increases, the carrying capacity of electric power cables decreases, a phenomenon that occurs more during the summer with the increase in electricity load caused by air-conditioning usage (Bartos et al., 2016). Moreover, UHI and heatwaves have a relevant environmental and financial impact, especially on vulnerable and low-income populations (Santamouris and Kolokotsa, 2015). Additionally, exposures to high ambient temperatures represent a serious health danger (Anderson G. Brooke and Bell Michelle L., 2011).

The urban climate is strongly determined by morphological characteristics and the properties of the materials comprising the urban landscape (Lemonsu et al., 2015). Many strategies focusing on new material developments have been proposed to mitigate the rise in cooling demand, and the increase in urban temperatures. Increasing the global albedo of the city has resulted in a reduction in the peak ambient temperature of up to 3 ºC and a 20% reduction in peak cooling demand in residential buildings (Santamouris et al., 2018). Cool roofs have been widely studied for reducing the cooling demand (Bell et al., 2003; Berdahl and Bretz, 1997; Erell et al., 2006; Kolokotroni et al., 2013; Kolokotsa et al., 2018; Miller et al., 2015; Radhi et al., 2017; Santamouris, 2013; Santamouris et al., 2008). Green roofs and vegetation have been proposed as a mitigation strategy as well (Foustalieraki et al., 2017; Herrera-Gomez et al., 2017; Kolokotsa et al., 2013; Zinzi and Agnoli, 2012).

Recently developed radiative cooling materials have achieved daytime sub-ambient temperatures even under direct solar radiation. Radiative cooling is the physical phenomenon by which an object dissipates heat as infrared radiation. Over mid-infrared wavelengths, between 8 and 14 μm, the Earth's atmosphere is transparent to electromagnetic radiation. Radiative cooling was applied as a nocturnal passive system for cooling in some experimental buildings and prototypes (Yellot, 1976; Yellot, John I., 1976). The results showed a limited nocturnal cooling capacity since longwave radiation from commonly-found materials can rarely achieve cooling powers of more than 100 $W\cdot m^{-2}$, even under ideal meteorological conditions (Erell and Etzion, 1992). Material sciences have significantly evolved since the first designs were researched in the early '70s and radiative cooling materials have recently been developed (Kou et al., 2017; Li et al., 2017; Raman et al., 2014; Rephaeli et al., 2013; Shi et al., 2018; Zhai et al., 2017; Zhu et al., 2019, 2015). Novel materials such as photonics, metasurfaces, and polymers have already achieved 120 $W\cdot m^{-2}$ under direct sunlight (Santamouris and Feng, 2018). Besides material development, aperture dependency and geometrical designs have been studied. This kind of device was introduced by Trombe in 1967 (cited by (Smith, 2009)) by placing blackbody materials facing the sky and protecting them from the environment. Several authors have continued this line of research (Aviv and Meggers, 2017; Smith, 2009; Zhou et al., 2019a, 2019b), showing temperature drops of up to 11 ºC below ambient temperature.

In order to achieve daytime radiative cooling, the optical properties in each wavelength of a material are determinant. The material needs to emit highly in the atmospheric transparency window (7.9-14 μm) and reflect at least 94% of incident sunlight (0.3-3 μm) (Raman et al., 2014). Absorbing 10% of incident solar radiation is approximately 100 $W \cdot m^{-2}$ and therefore, the thermal equilibrium is reached at a higher temperature than the ambient temperature. Daytime radiative cooling materials have been coupled to air-conditioning (AC) systems to evacuate the excess heat to space instead of to the ambient air (Aili et al., 2019; Goldstein et al., 2017; Wang et al., 2018; Zhang et al., 2018). In (Zhao et al., 2019), the authors compared an air radiative cooling system with other materials and systems (shingle roof, attic ventilation, and coolroof). Using their proposed radiative cooling system, they achieved a reduction in the attic air temperature of 15.5-21 ºC. Another system using the material developed by (Zhai et al., 2017) reduced the energy consumption and achieved savings from 26% to 46% for the modeled locations (Zhang et al., 2018).

Radiative cooling depends on the optical properties of the material and the thermal exchange with the surroundings. The effect of climatic parameters such as the effect of air temperature, solar radiation, and ambient radiation have recently been discussed (Feng et al., 2020). Moreover, the contribution of convection has been vastly researched (Chen et al., 2016; Cui et al., 2016; Huang and Ruan, 2017; Kou et al., 2017). Various studies have calculated the radiative cooling potential of several devices and materials in different cities (Feng et al., 2020; Vall et al., 2018), countries (Li et al., 2019), and areas of the world (Argiriou et al., 1992). Nevertheless, a more detailed study showing the impact of the optical properties of each wavelength band on the ability to achieve sub-ambient cooling has not yet been presented.

This research aims to study the impact of the different spectral selectivity configurations in the cooling potential of radiative materials by conducting a sensitivity analysis. The effects of each wavelength's band emissivity on the ability to achieve sub-ambient cooling was determined. The authors compared the performance of several theoretical radiative cooling materials with newly developed ones and typical construction materials. The materials were studied under two conditions to assimilate a passive and active solution (for future integration in AC systems). Firstly, the passive solution was designed as a highly insulated surface on one side (an almost adiabatic condition). Secondly, the active condition was assimilated to a very conductive surface. Besides, several convective values were simulated to determine the maximum sub-ambient cooling. As a result, considerations for choosing the appropriate spectral emissivity configuration are given for each location. The restrictions to achieving daytime radiative cooling are detailed for both conditions.

The main novelty of this study is that it shows that the desired spectral emissivity characteristics of radiative cooling materials depend on the climate conditions and the type of application. It was discovered that the best spectral characteristics are different for a dry or humid climate and if the application is for a passive system or an active one. In-depth study of these two aspects is required in future research to establish the level of importance of these two observations using broader statistical data.

2. Methodology

The research methodology described was followed to determine the impact of the spectral emissivity configuration on the possibility of achieving sub-ambient temperatures. First, a heat transfer model was developed. This model simulated a horizontal flat plate, in which the conductive heat transfer was calculated using the finite difference method (implicit method). The boundary conditions on the lower side were convection and the temperature of a fluid. For a highly insulated condition, a nearly zero value is defined for the convective heat transfer coefficient. For the upper side, the boundary conditions defined were convection with air, incident solar radiation, and radiation exchange with the atmosphere. The optical properties varied spectrally, and the model considered this variation for both solar radiation and atmospheric radiation. Atmospheric radiation is based on the spectrally selective sky model presented by Berger and Bathiebo (Berger and Bathiebo, 1989), where the sky conditions were defined as clear sky, completely covered sky, and partially covered sky.

The model can perform transient and steady-state simulations with time steps specified at the beginning of each simulation (for this study, a 1-minute time step was used in all cases); the summary results presented are hourly, however. The main variables obtained in the results are surface temperatures and heat transfer on the surface. The heat transfer is discretized for each transfer mechanism: conduction, convection, radiation from the atmosphere, and solar radiation absorption. The power at the end of the hour is given for each heat transfer mechanism. Moreover, the cumulative energy transferred during the hour is presented. The previous results are used to obtain other related parameters, such as the hourly difference between air temperature and surface temperature, the daily mean of this difference, daily mean temperatures, and cumulative daily heat transfer.

The model was validated using outdoor experimental data from two newly developed radiative cooling materials (Raman et al., 2014; Zhai et al., 2017). Following the validation, the sensitivity analysis was conducted with 90 theoretical materials and seven existing materials in two locations: Sydney, with a mild climate and Phoenix, with an arid climate (Cfa and Bsh respectively according to (Kottek et al., 2006)). Moreover, the two boundary conditions—a high insulated and a very conductive surface—were simulated. Finally, the results are compared according to their radiative cooling potential and the surface temperature they reached. The suitability, restrictions, and limitations for each are presented for each location and boundary condition.

2.1. Heat transfer model

The objective of the heat transfer model is to simulate the thermal behavior of a horizontal surface that exchanges heat with its surroundings by convection and radiation. Radiation is divided into two components: solar radiation and radiation with the surroundings. The surrounding radiation will be assumed to be only from the sky. The heat transfer model calculated the heat transferred by conduction from the surface down with the finite difference method. The emphasis of the model is on the two radiation components, since it considers the spectral characteristics of the surface, sky and solar radiation; therefore, only this component will be explained.

The radiosity of a surface with a view factor equal to one with the sky can be represented by:

$$J_s(v) = \varepsilon_s(v)E_b(v,T_s) + \left(1 - \varepsilon_s(v)\right)G_s(v) \quad (1)$$

Where $J_s(v)$ is the radiosity of the surface for the wavenumber v, $\varepsilon_s(v)$ the emissivity of the surface for the wavenumber v, $E_b(v,T_s)$ the blackbody radiation in the wavenumber v when its temperature is T_s, $G_s(v)$ the irradiance received by the surface at a wavenumber v.

As the sky is the only radiation emitter that the surface faces, the irradiance received by the surface is:

$$G_s(v) = \varepsilon_{sky}(v)E_b(v,T_{air}) \quad (2)$$

Therefore:

$$J_s(v) = \varepsilon_s(v)E_b(v,T_s) + \left(1 - \varepsilon_s(v)\right)\varepsilon_{sky}(v)E_b(v,T_{air}) \quad (3)$$

On the other hand, the radiation heat flux in the surface for the wavenumber v is:

$$q_{r,s,v} = J_s(v) - G_s(v) \quad (4)$$

$$q_{r,s,v} = \varepsilon_s(v)\left(E_b(v,T_s) - \varepsilon_{sky}(v)E_b(v,T_{air})\right) \quad (5)$$

For the wavelength bands between wavenumbers between v_i and v_j the heat flux is:

$$q_{r,s,\Delta v} = \int_{v_i}^{v_j} \varepsilon_s(v) \left(E_b(v, T_s) - \varepsilon_{sky}(v) E_b(v, T_{air}) \right) dv \quad (6)$$

$$q_{r,s,\Delta v} = \int_{v_i}^{v_j} \varepsilon_s(v) E_b(v, T_s) dv - \int_{v_i}^{v_j} \varepsilon_s(v) \varepsilon_{sky}(v) E_b(v, T_{air}) dv \quad (7)$$

Selecting a range or band Δv where both $\varepsilon_s(v)$ and $\varepsilon_{sky}(v)$ can be considered approximately constant yields the following expression:

$$q_{r,s,\Delta v} = \varepsilon_{s,\Delta v} \left[\int_{v_i}^{v_j} E_b(v, T_s) dv - \varepsilon_{sky,\Delta v} \int_{v_i}^{v_j} E_b(v, T_{air}) dv \right] \quad (8)$$

The previous equation makes it possible to calculate the heat flux exchanged by radiation with the sky for each band in which the emissivity of the sky and the surface can be considered constant. The total heat flux is therefore the summation of the heat flux of each band:

$$q_r = \sum_{\Delta v_i} q_{r,s,\Delta v_i} \quad (9)$$

The second component of radiation is the solar radiation. In this case the heat can be calculated with:

$$q_{sun} = \int_0^\infty \varepsilon_s(v)\, I(v) dv \quad (10)$$

And similar to the previous considerations, if there are bands where emissivity can be considered as constant, the previous integral can be approximated by a summation:

$$q_{sun} \approx \sum_{\Delta v_i} \varepsilon_{s,\Delta v_i}\, I_{\Delta v_i} \quad (11)$$

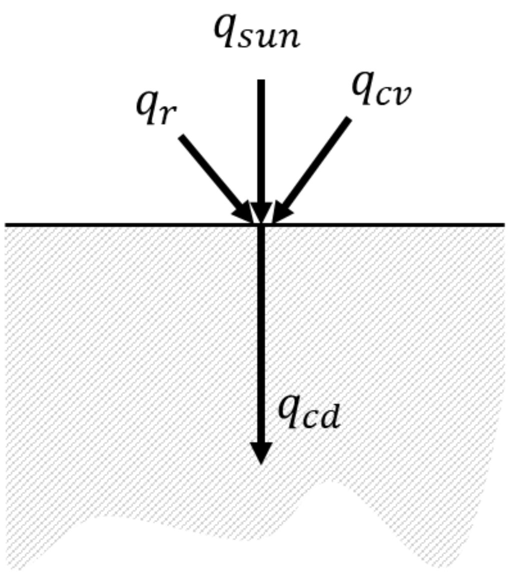

Figure 1. Heat flux in the surface

Finally, the balance of heat flux at the surface, following the schematic representation of Figure 1, can be expressed as:

$$q_{cd} = q_r + q_{sun} + q_{cv} \tag{12}$$

Where:

$$q_{cv} = h_{cv}(T_{air} - T_s) \tag{13}$$

And q_{cd}, as stated above, is calculated using the finite difference method.

2.1.1. Sky model review and development

Calculating the heat transfer with the atmosphere using equation 8 requires the spectral emissivity of the sky ($\varepsilon_{sky,\Delta v}$) to be known.

Although there is a vast literature on sky models (30 evaluated in (Vall and Castell, 2017), 35 in (Algarni and Nutter, 2015) and 70 in (Antonanzas-Torres et al., 2019)) both for clear sky conditions and cloudy conditions, most of them refer to global emissivity. Clouds act as a barrier to heat transfer, inhibiting the outgoing radiation through the atmospheric band and augmenting the effective temperature of the sky due to the absorption of heat by water vapor (Berdahl and Fromberg, 1982). Opaque clouds can be considered blackbody emitters at the temperature of the cloud base (Bliss, 1961) and their radiative effect close to the transparency window. The influence of cloud radiation decreases with altitude; higher clouds are colder than lower clouds (Sugita and Brutsaert, 1993). Nevertheless, measurements of the downward component emitted by clouds and aerosols in the atmosphere are scarce and not well understood (J Herrero and Polo, 2012).

Cloudy sky models are based on daytime clearness indexes and are transposed as a single value for the night; moving clouds cannot be considered (Eicker and Dalibard, 2011). Moreover, at night there are no cloud coverage estimations. Malek (Malek, 1997) proposes a method to evaluate sky cloud cover without having to relate to any empirical and local constants. It is based on the cloud base height, cloud base temperature, and percentage of the sky covered by clouds. Emissivity value estimates are 1 under cloudy conditions (Martin and Berdahl, 1984) and above 0.95 for covered skies (J. Herrero and Polo, 2012) . According to (Monteith and Unsworth, 2013), for a completely overcast sky (cloud fraction *c = 1*) in Oxford, England, the apparent emissivity of the sky can be calculated knowing the emissivity value for clear sky by:

$$\varepsilon_{sky,cloud} = \varepsilon_{sky}(1) = 0.84 + 0.16\varepsilon_{sky,clear} \quad (14)$$

And for a sky covered with a fraction “*c*” of cloud, emissivity can be calculated by interpolation:

$$\varepsilon_{sky}(c) = c\varepsilon_{sky}(1) + (1 + c)\varepsilon_{sky,clear} \quad (15)$$

Clear sky emissivity model

This research uses the Berger and Bathiebo 1989 (Berger and Bathiebo, 1989) spectral sky model to calculate the spectral radiation of the atmosphere. The model calculates the spectral and global emissivity of the sky in 21 wavelength ranges, using Equation 16

$$\varepsilon_{sky,\Delta v_i} = 1 - exp\left(-k_{\Delta v_i} w_j\right) \quad (16)$$

Where $\varepsilon_{sky,\Delta v,i}$ is the clear sky emissivity for the range of wavenumbers Δv_i; $k_{\Delta v,i}$ is an absorption coefficient, and w_j an equivalent absorber that must be calculated using different correlations defined by (Berger and Bathiebo, 1989) for each band.

Completely covered sky emissivity

To the best knowledge of the authors, there are no correlations to calculate the spectral emissivity under completely covered skies with a similar degree of discretization that has been presented for clear skies. The model developed can calculate the emissivity of the sky using a correlation of Equation 14 or a constant value. By default, a value of 0.95 (J. Herrero and Polo, 2012) was used for the results calculated in this paper.

Partially covered sky emissivity

As shown in Equation 15, a linear relationship between the emissivity of clear skies and completely covered skies is presented in (Monteith and Unsworth, 2013). This principle can be applied for each spectral band. The parameter "c" is used as the fraction of sky covered by clouds, 1 being a completely covered sky. For a sky covered with a fraction c of cloud, interpolation gives:

$$\varepsilon_{sky,\Delta v_i}(c) = c\varepsilon_{sky}(1) + (1 - c)\varepsilon_{sky,\Delta v_i} \quad (17)$$

The sky emissivity for a partially covered sky is the weighted average between the emissivity of clear sky and the completely covered sky, the ratio of the covered sky being the weighting factor. Note that emissivity for a completely covered sky $\varepsilon_{sky}(1)$ is not dependent on the wavenumber since there is no information about its spectral variation.

2.2. Model validation

The model was validated using data from two recently developed materials in the literature (Raman et al., 2014; Zhai et al., 2017); the authors reported very high cooling rates even when exposed to the sun and achieved a substantial temperature drop from the ambient temperature. The model agreed well with experimental data (Figure 2 and 3) and is considered valid.

Table 1: Comparison of the two radiative cooling materials under experimental conditions.

	Skycool (Raman et al., 2014)	**Radicool (Zhai et al., 2017)**
Solar Reflectivity	0.90	0.90
Emissivity in the transparency window	0.80	0.93
Reported sub-ambient temperature	4.9 ºC	
Cooling potential	40.1 W/m^2	93 W/m^2
Location of experiment	Stanford, CA, USA	Cave Creek, AZ, USA
Köppen climate exp	Csb	BSh
Dates of the experiment	Clear winter day	16^{th} Oct. to 19^{th} Oct (Fall)

In the experiment conducted in 2014, the authors exposed the radiative cooling material protected by a low-density polyethylene cover to the sky. These polyethylene covers acted as a convection barrier (See Supplementary Material 1: Model Validation Procedure).

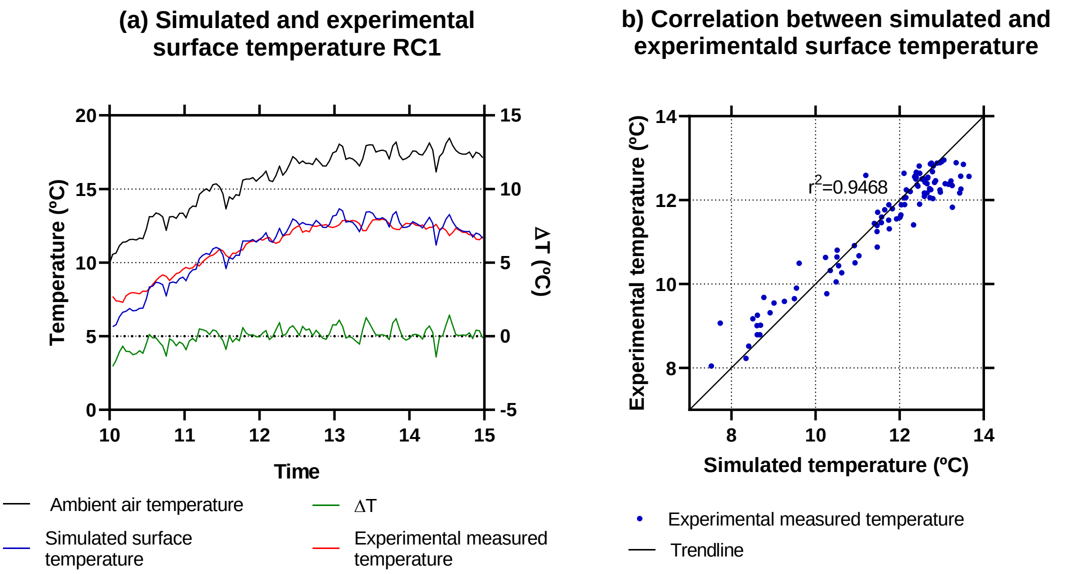

Figure 2. Validation of the thermal model with material 1 (RC1) "Skycool" (Raman et al., 2014).

The second experimental setting was different; they eliminated convection by applying a constant heat supply to the material to achieve ambient temperature.

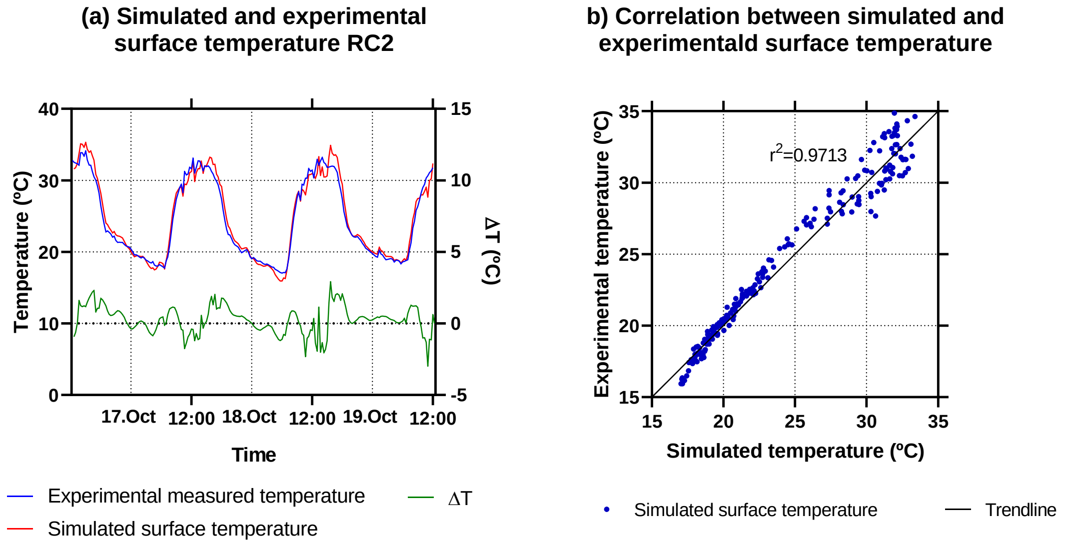

Figure 3. Validation of the thermal model with material 1 (RC2) "Radicool" (Zhai et al., 2017).

2.3. Sensitivity analysis

The objective of this sensitivity analysis was to determine the impact of wavelength emissivity on the ability to achieve daytime radiative cooling. The radiation spectrum was divided into 39 bands (See Supplementary Material 2: Band division), parting from the original 21 wavelength bands from the atmospheric radiation model (Berger and Bathiebo, 1989).

An emissivity value of zero or non-zero was assigned to each band; fifteen wavelength combinations were proposed. To establish the bandwidth for an ideal material, the non-zero emissivity values of the theoretical materials were selected to be centered in the transparency window of the atmosphere (infrared emission), shown in Figure 5. Similarly, for the visible region, the emissivity values were centered in the region with the highest solar irradiance. The band combinations resulted in the 15 theoretical materials (M1-M15) shown in Figure 4. Moreover, to quantify the impact of the emissivity value, six emissivity values (1, 0.9, 0.8, 0.7, 0.5, and 0.25) were assigned to the non-zero value, resulting in a total of 90 theoretical materials.

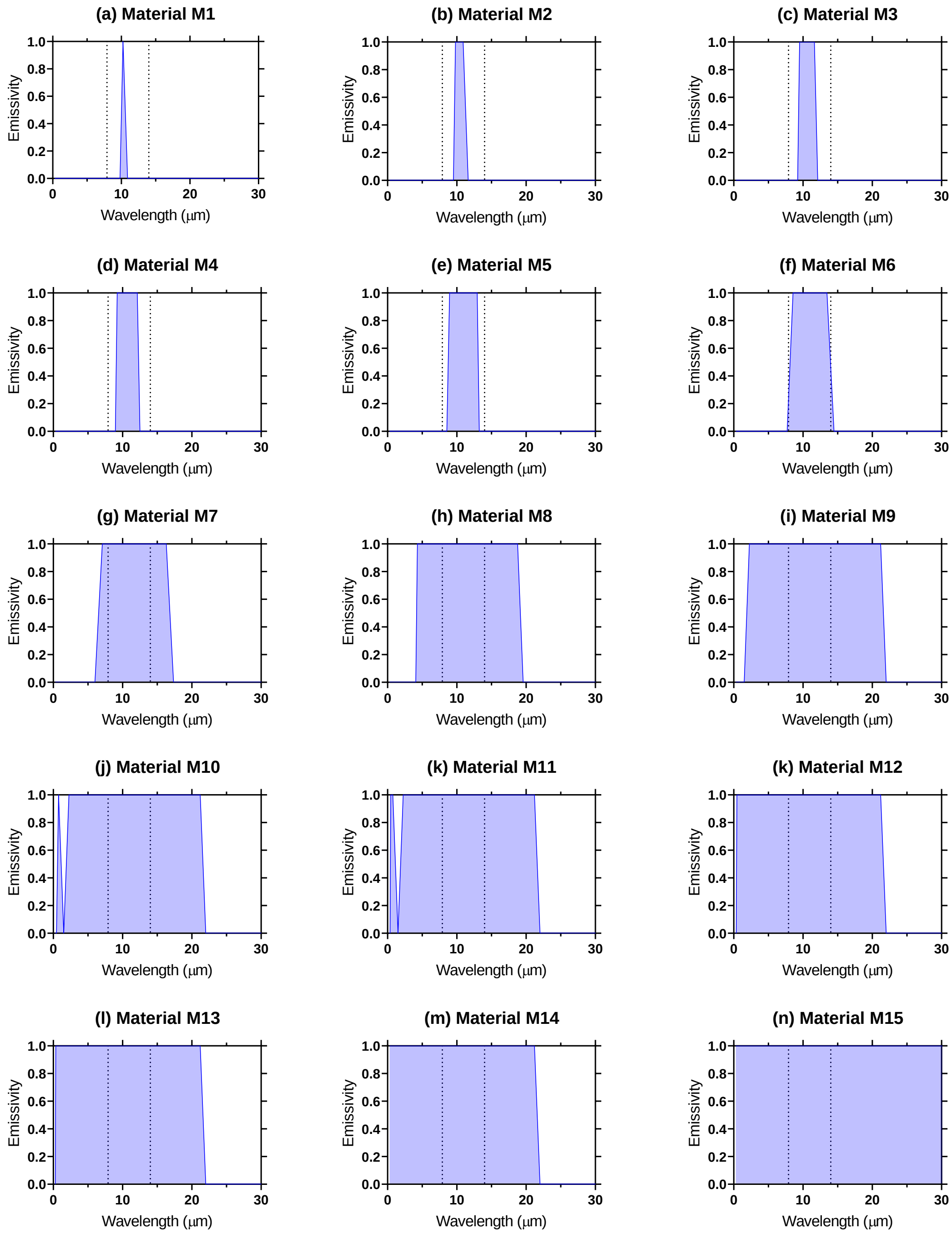

Figure 4. Emissivity of the theoretical materials (M1-M15) resulting from combining emissivity values of 1 and 0 in the 39 wavelength bands.

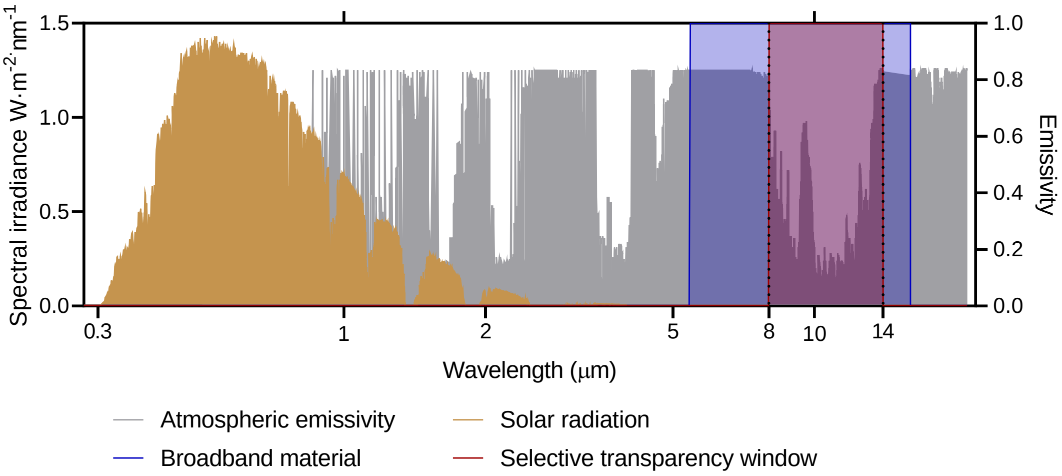

Figure 5. Solar spectrum, atmospheric emissivity, and ideal material spectra.

The performance of the theoretical radiative cooling materials (M1-M15) was compared with existing radiative cooling materials (Skycool (RC1) and Radicool (RC2)) and other construction materials (CM1-CM5 e.g. white paints, brick, and coolmaterials) for the same boundary conditions. This provides a better understanding of the potential benefits and ways to improve these materials.

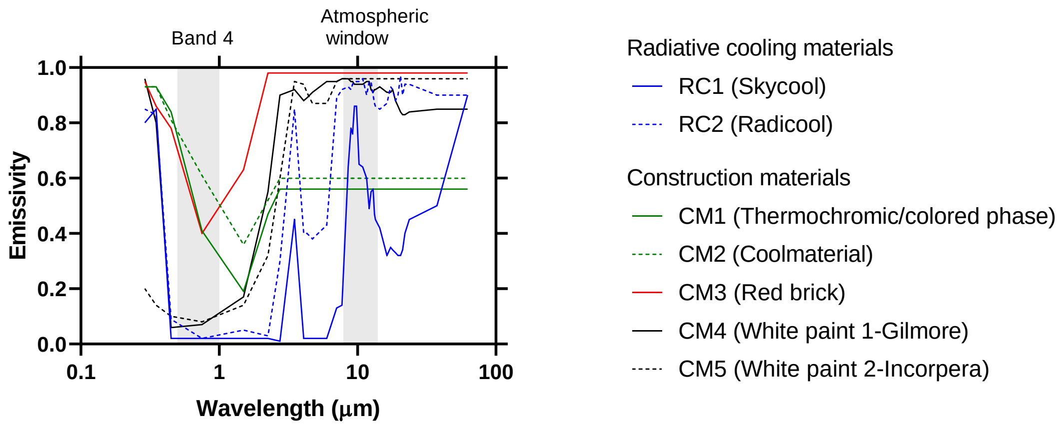

Figure 6. Emissivity comparison of existing radiative cooling materials (RC) and construction materials (CM).

The sample's thermal response was calculated in two different cities, Phoenix (hot and dry) and Sydney (mild and humid) during the summer solstice, on 21st June and 21st

December, respectively. The climates of the selected cities obtained from Meteonorm (*Meteonorm 7*, 2017) represent completely clear skies and are shown in Figure 7.

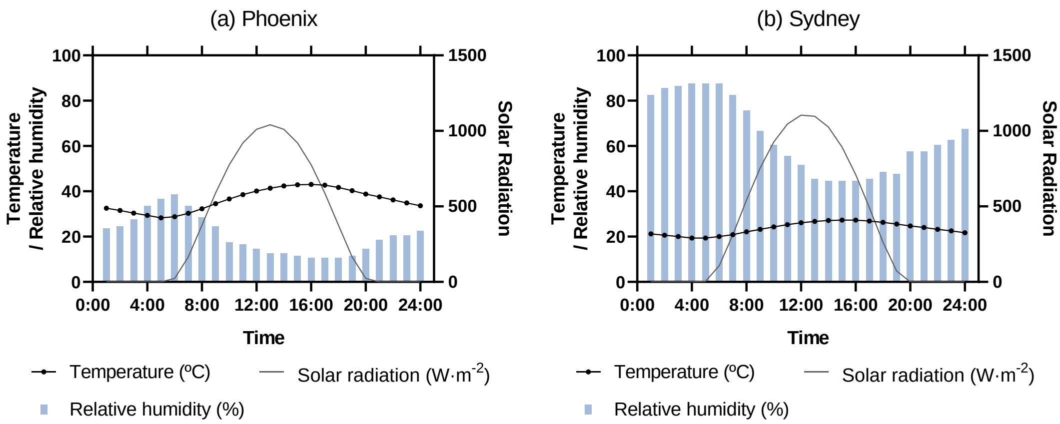

Figure 7. Hourly climatic parameters in summer solstice for Phoenix and Sydney.

3. Results

Two different simulation conditions were considered: a highly insulated and a very conductive surface (Table 2).

Table 2: Material substrate for two conditions

Background conditions	Material	Thickness	Thermal conductivity	Density	Specific Heat
1. Insulated	Insulation	0.15 m	0.0001 W/m·K	0 kg/m3	1000 J/kg·K
2. Conductive	Metallic sheet	0.005 m	400 W/m·K	0 kg/m3	1000 J/kg·K

3.1. Performance of the samples over a highly insulated surface

The first thermal scenario considers the material insulated entirely on the bottom side to have almost no conductivity; there is negligible heat transfer by conduction. Therefore, this condition can be regarded as almost adiabatic. Below the insulation, the temperature was 25 ºC, and the exterior convective heat transfer coefficient was 20

W·m^{-2}·K^{-1}. In this case, the resulting variable of interest is the surface temperature reached.

To study the effect of each of the 39 bands, the emissivity value in the selected band was 1 and 0 in the rest of the 38 bands. As Figure 8 shows, from “Band 2” (0.3-0.4 µm) to “Band 7”(2.5-3 µm), having an emissivity of 1 leads to heat gains, especially in “Band 4” (0.5-1 µm), where the material is 10.57 ºC and 9.90 ºC hotter than the ambient temperature in Sydney and Phoenix, respectively. On the other hand, “Band 15” (8.29-8.82 µm) and “Band 20” (9.98-10.50 µm) to “Band 22” (11.33-11.95 µm) have a high impact on the heat losses, reaching a reduction of 1.13 ºC in Phoenix and 0.88 ºC in Sydney when the emissivity of “Band 21” (10.5-11.325 µm) equals 1. Absorbing heat in the solar wavelengths has a more significant effect than the emissive power inside the atmospheric window, as can be seen in Figure 8.

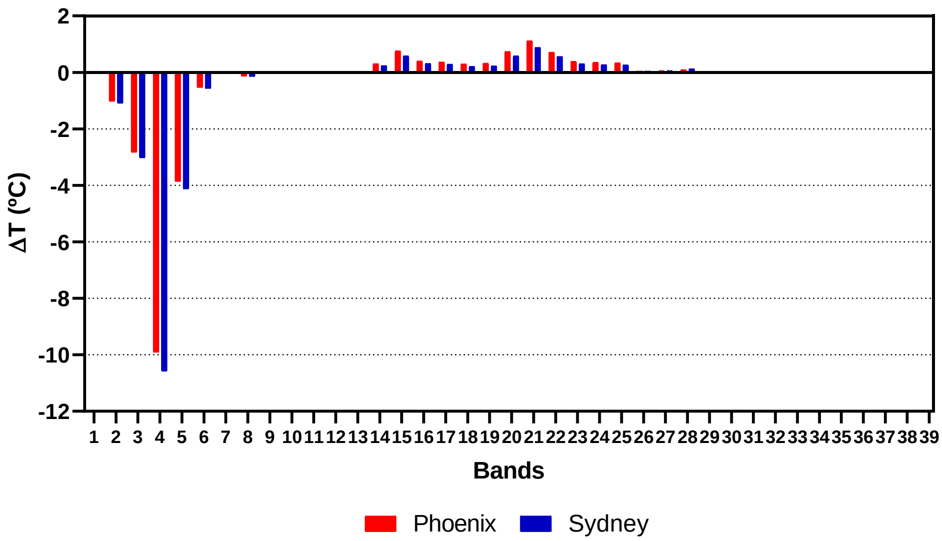

Figure 8. Contribution of each band’s emissivity to the average temperature difference. Positive values are bands that achieved sub-ambient cooling and negative values are those that reached higher than ambient temperatures.

Once the effect of each band was known, the surface temperature of the 15 theoretical materials was calculated with the six possible emissivity values and the existing materials (Figure 9). The results for the theoretical materials were divided into two groups: those that achieved sub-ambient cooling during the day (M1-M9, Figure 9 a1, b1), and the ones that reached higher than ambient temperatures (M10-M15, Figure 9 a2, b2). All the materials achieved higher temperature reductions in Phoenix than in Sydney. M6 achieved a 5.29 ºC reduction in Phoenix and M7 a reduction of 4.20 ºC in Sydney (see Figure 10 a1, b1), whereas RC2 reached a mean temperature drop of 3.42 ºC in Phoenix and 2.36 ºC in Sydney. CM5 achieved a very similar temperature reduction, 3.12 ºC, and 2.05 ºC, respectively. The thermochromic paint (CM1), the cool material (CM2), and the red brick (CM3) did not achieve sub-ambient temperatures during the day (Figure 9 c, d).

Lowering the emissivity of the theoretical materials led to a reduction in the attained surface temperature, as seen in Figure 10 (c, d); however, a material with an emissivity of 0.25 in the atmospheric window and 0 outside achieved a temperature reduction of 1.51 ºC in Phoenix and 1.17 ºC in Sydney. During the night, all the studied materials, theoretical and existing, achieved sub-ambient cooling.

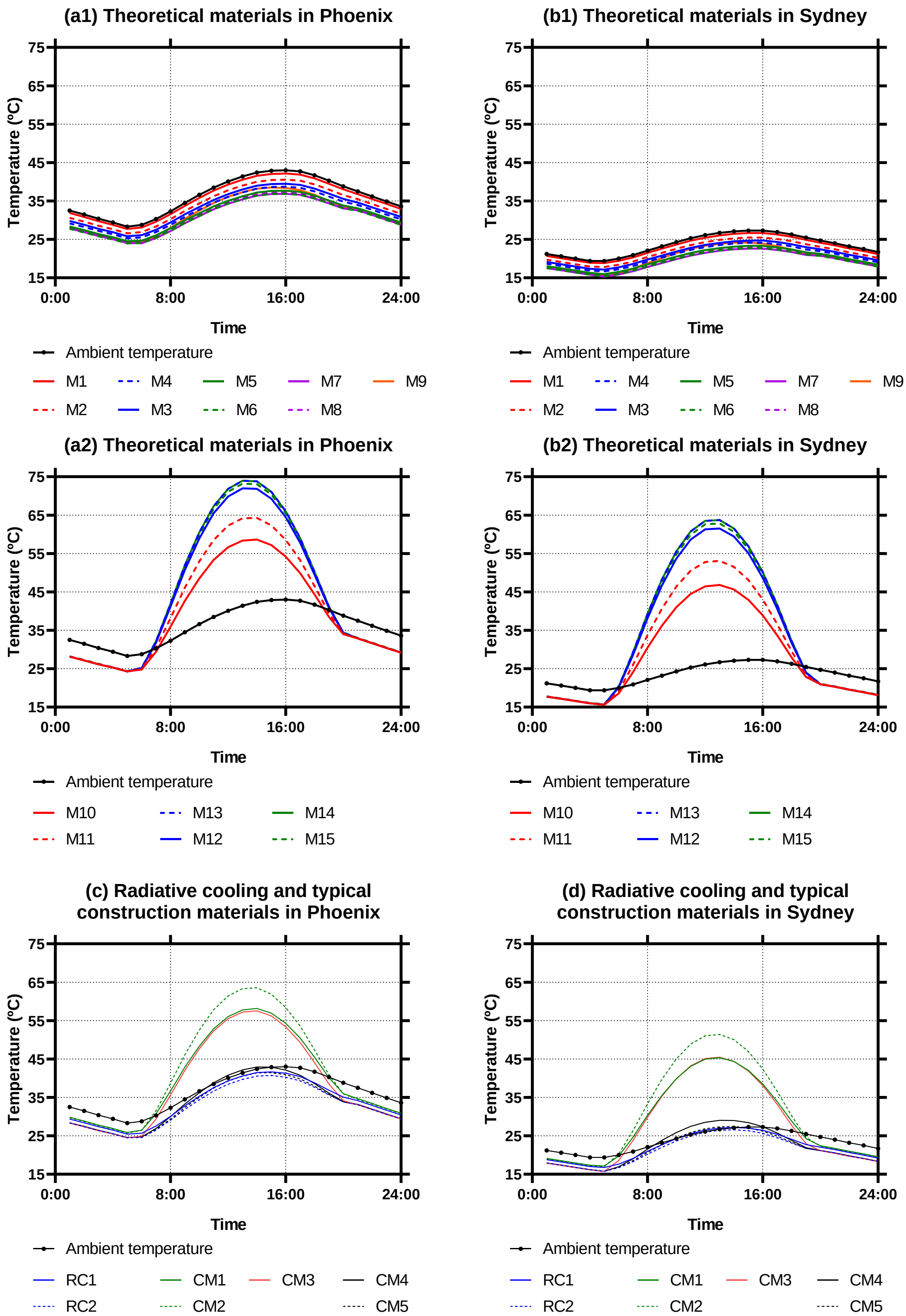

Figure 9. Hourly surface temperature achieved by the materials in Phoenix and Sydney.

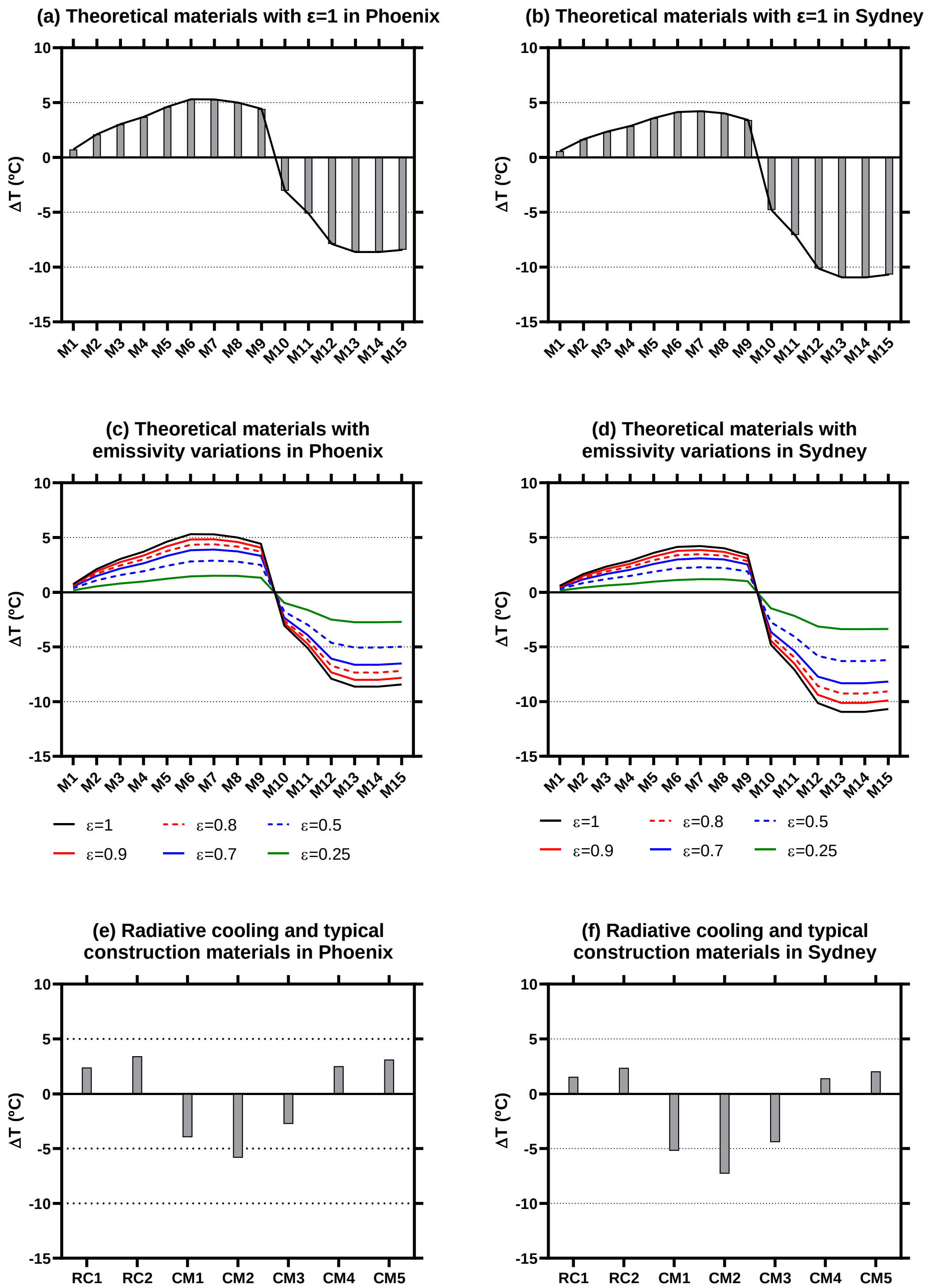

371

372 *Figure 10. Difference between mean ambient and surface temperature for theoretical materials*

373 *(M1-M15), radiative cooling materials (RC1-RC2) and typical construction materials (CM1-CM5)*

in Phoenix and Sydney. Positive values are materials that achieved sub-ambient cooling and negative values higher than ambient temperatures.

Figures 9 and 10 above show summarized behavior and a comparison of the simulated materials considering a highly insulated condition. If the objective is to achieve the minimum surface temperature, the ideal material is M6 for Phoenix and M8 for Sydney. Nevertheless, in both cases (mainly for Phoenix), the difference between M6 and M8 is low. Therefore, the ideal material should have an emissivity of 1 approximately in the band between 5 and 17µm. The emissivity in the visible region has a powerful impact on the behavior of the material since the infrared emission cannot be compensated by solar absorption. The emissivity of the white paints (CM4 and CM5) was very similar to “Skycool” and “Radicool” (RC1 and RC2), and therefore their thermal behavior is similar to radiative cooling materials.

Finally, in order to study the effect of the convective coefficient, the mean surface temperature achieved by M1 to M15 was calculated and is shown in Figure 11. When the convection is reduced, Phoenix (M6, 37 ºC) had the potential to achieve a lower sub-ambient temperature than Sydney (M6, 31 ºC). On the other hand, a lower convective rate led to a higher surface temperature in Sydney (M15, 31 ºC) than in Phoenix (M15, 23 ºC).

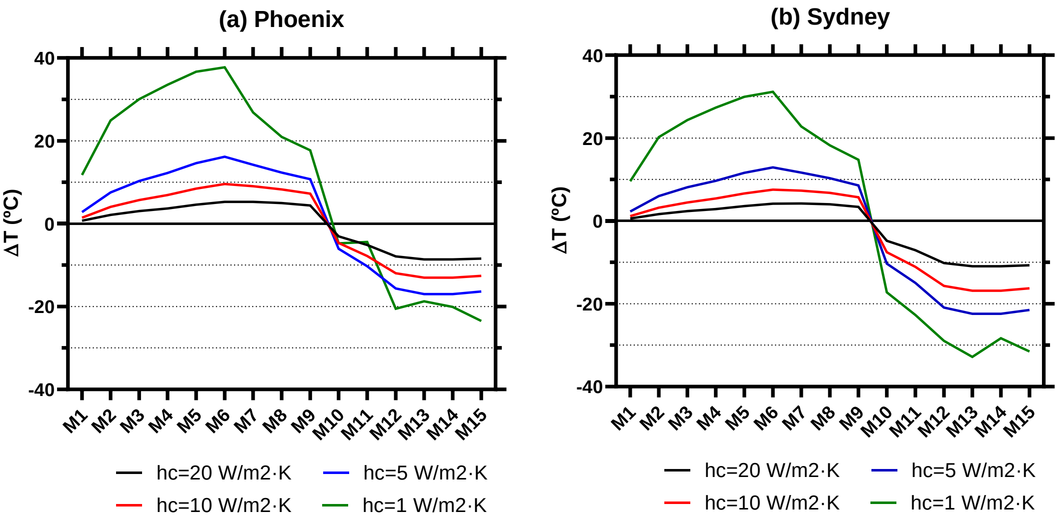

Figure 11. Difference between mean ambient and surface temperature for theoretical materials (M1-M15) with different convective values in Phoenix and Sydney. Positive values mean sub-ambient cooling and negative values higher than ambient temperatures.

3.2. Performance of the samples over a conductive surface

In the second scenario, materials are placed on top of a very conductive surface with no insulation. This scenario mimics the idea of having a fluid or a heat source at a constant temperature under the surface and calculates the cooling potential. Below the material, the temperature is 25 ºC, the exterior heat transfer coefficient is 25 W·m^{-2}·K^{-1}, and the interior heat transfer coefficient is 1000 W·m^{-2}·K^{-1}.

The daily heat gains were calculated for all the materials in both cities and are represented in Figure 12. In the case of Phoenix (Figure 12 a), using a very conductive material leads to heat gains since the mean ambient temperature that day is 36.19 ºC. Nevertheless, the theoretical material M6 with an emissivity of 1 achieves the lowest heat gain of 3091 Wh·m^{-2}, followed by M7 (3306 Wh·m^{-2}) and M5 (3384 Wh·m^{-2}). Among the existing materials, the behavior of RC2 (4578 Wh·m^{-2}) and CM4 (5240 Wh·m^{-2}) is closer to that of RC1 (4645 Wh·m^{-2}) and CM5 (4897 Wh·m^{-2}). The mean ambient temperature in Sydney for that day is 23.6 ºC (Figure 12 b). Materials M1-M9 achieved a substantial heat loss: theoretical material M8 attained the highest heat loss of -3176 Wh·m^{-2} followed by M7 (-3140 Wh·m^{-2}), and M6 (-2916 Wh·m^{-2}), when the emissivity value is 1 (Figure 12 b).Among the existing materials, the highest heat losses correspond to RC1 (-2212 Wh·m^{-2}) and CM5 (-2077 Wh·m^{-2}). Contrary to the situation in Phoenix, despite having similar optical properties to RC1 and CM5, materials RC2 and CM4 achieved values that were around 700 Wh·m^{-2} lower.

In the case of Phoenix (Figure 12 c), reducing the emissivity of the theoretical materials M1 to M9 leads to higher heat gains. Material M6 attains the best behavior since it has the lowest heat gains. Once the materials start to absorb in the solar wavelengths, the higher the emissivity, the greater the heat gains are. In the case of Sydney (Figure 12 d), reducing the emissivity of the theoretical materials leads to lower heat losses for M1 to M9. Material M8 attains the best behavior as it has the highest heat losses.

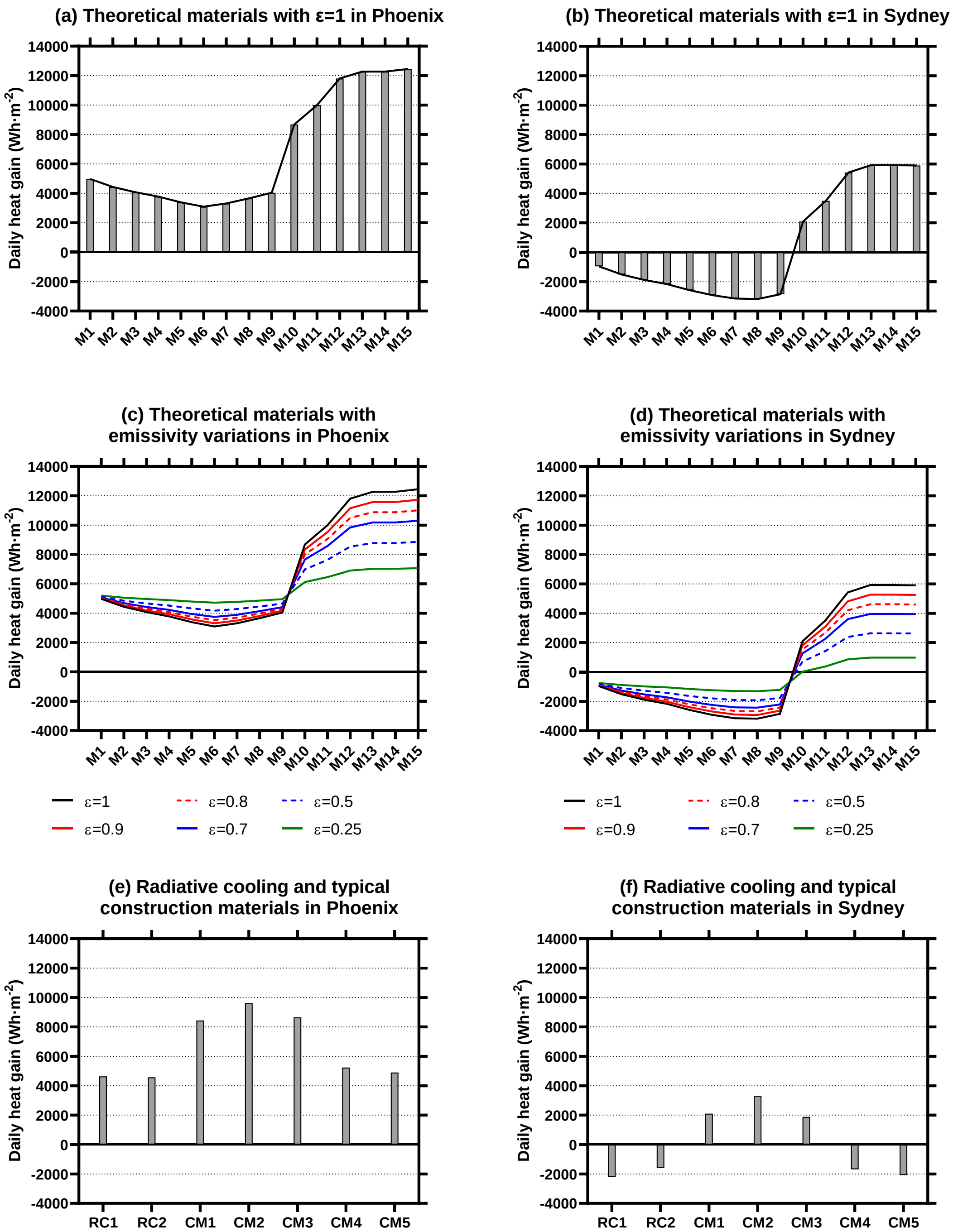

Figure 12. Daily gains or losses for theoretical materials (M1-M15), radiative cooling materials (RC1-RC2) and typical construction materials (CM1-CM5) in Phoenix and Sydney. Positive values are heat gains and negative are heat loses.

The daily accumulated radiated heat of each surface is represented in Figure 13. As can be seen, the potential is higher in Sydney than in Phoenix due to the difference in the ambient temperatures of both cites; that the bottom surface is at 25 ºC hinders enormously the cooling ability in Phoenix, where M6 attains the highest radiation power, -2218 Wh·m^{-2}· (Figure 13 a). The difference between using one of the theoretical materials and the already developed ones is substantial, the radiated heat almost halving in the latter (Figure 13 e). RC2 achieved -1475 Wh·m^{-2}and CM5 -1359 Wh·m^{-2}. In the case of Sydney (Figure 13 b), from M7 (-2517 Wh·m^{-2}) onwards, all the materials achieve a similar radiation power. In this case, RC2, and RC5 achieve -2398 Wh·m^{-2}, -2484 Wh·m^{-2}, respectively. In both cities, lowering the emissivity leads to lower radiated heat (Figure 13 c, d). When the exchange temperature is higher, the theoretical radiative cooling materials perform better, as shown in Phoenix.

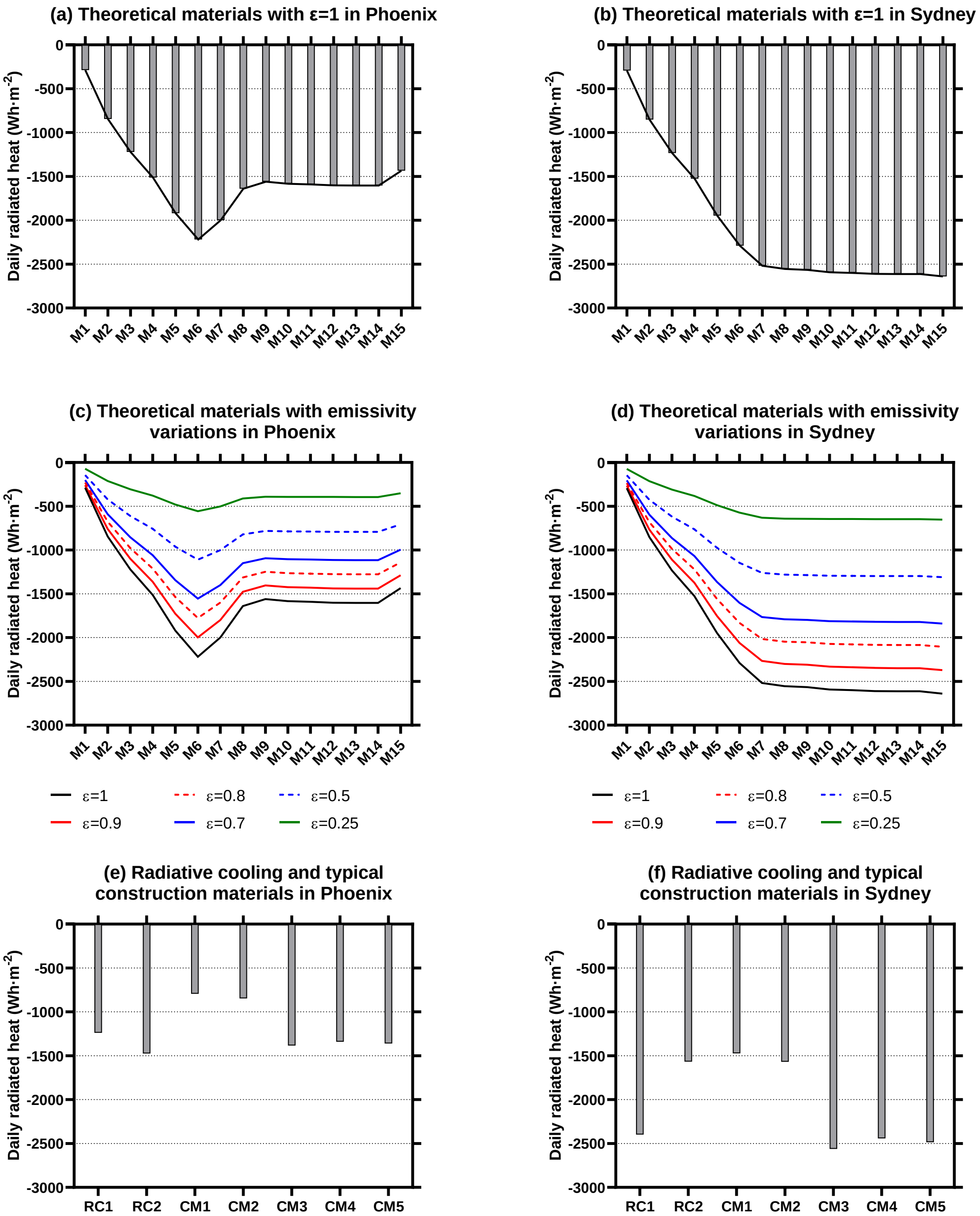

Figure 13. Daily radiated heat for theoretical materials (M1-M15), radiative cooling materials (RC1-RC2) and typical construction materials (CM1-CM5) in Phoenix and Sydney. Positive values are heat gains and negative are heat loses.

Finally, to study the effect of the convective coefficient, the thermal gains for materials M1 to M15 were calculated and are shown in Figure 14. As mentioned above, the mean ambient temperature of Phoenix is higher than the interior temperature considered. Therefore, in this case, the higher the convection, the lower the cooling capacity in Phoenix; the air temperature heats the surface leading to considerable heat gains. Convection plays a less significant role in Sydney since the interior temperature is closer to the ambient temperature.

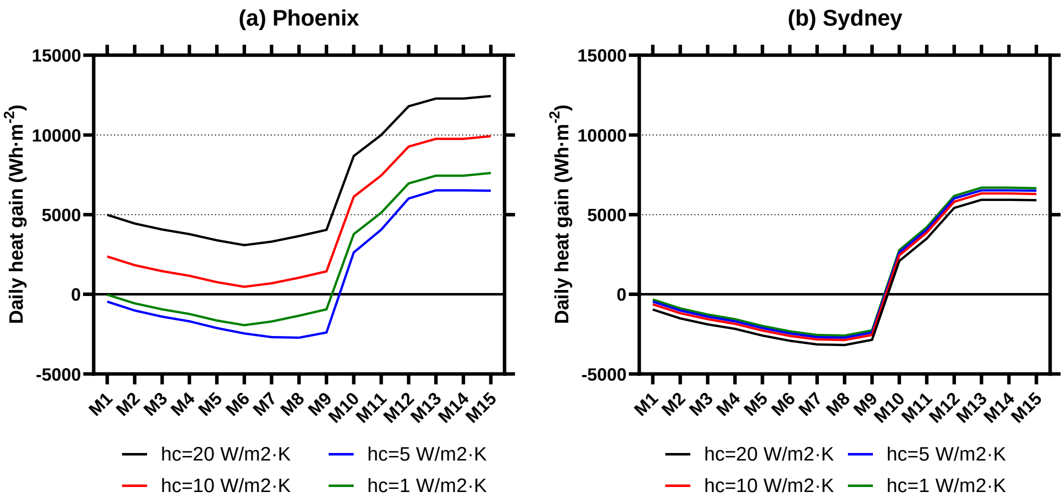

Figure 14. Daily gains or losses for theoretical materials (M1-M15) with different convective values in Phoenix and Sydney. Positive values are heat gains and negative are heat loses.

4. Conclusions

This paper analyzes the sensitivity of the performance of daytime radiative cooling materials to different spectral selectivity configurations, type of application, and location. The results presented in this paper suggest that the kind of application (active or passive) is a determinant factor in the design of radiative cooling materials. A material that performs well in a dry climate as a passive solution could perform poorly as an active solution. When used as an active solution, the operating temperature and climate should be carefully studied.

The radiation spectrum was divided into 39 bands and the contribution of each band was calculated. The most critical bands regarding heat absorption are band 4 (0.5-1 µm) followed by band 5 (1-2 µm) and band 3 (0.4-0.5 µm). A material that solely emits in band 4 reaches a surface temperature up to 10.6 ºC higher than the ambient temperature in Sydney and 9.9 ºC in Phoenix. Therefore, it is important to achieve high reflectivity in the 0.5-1 µm region. The emissivity values should be especially high in Bands 20-22 (9.98-11.95 µm). Combining the 39 bands, a total of 15 theoretical materials with 6 different emissivity values were proposed and compared to existing daytime radiative cooling materials and typical construction materials. As many authors have previously mentioned, the results of the daytime radiative cooling materials could not be directly compared. However, the present research has made it possible to compare under the same conditions the results of theoretical materials (M1-M15) with two of the most innovative radiative cooling materials in recent years, "Skycool" RC1 and "Radicool" RC2.

Modifying the materials' optical properties leads to a substantial change in the heat gains or losses in an active system and the surface temperature reached as a passive application. The most suitable optical spectrum for a material is determined by the climate of each location (Sydney and Phoenix in this study) and the application type (boundary conditions). The highly insulated condition was more beneficial in Phoenix, where the theoretical materials achieved (M6, 5.30 ºC) a higher sub-ambient cooling temperature than in Sydney (M6, 4.21 ºC). On the other hand, the materials that did not present sub-ambient cooling during the day (M10-M15) showed worse behavior in Sydney than in Phoenix due to the higher humidity. M14 reached a surface temperature10.93 ºC higher than the ambient temperature in Sydney and 8.63 ºC higher than in Phoenix. Using a radiative cooling material over a very conductive surface requires a different approach. In Sydney, a broader spectrum outside the atmospheric window was more beneficial than one solely within the transparency window. The theoretical material M8 achieved the highest daily heat losses (-3176 $Wh \cdot m^{-2}$). In this case, the existing materials RC1 and CM5 are good alternatives to the theoretical materials. In Phoenix, on the other hand, restricting the emissivity to the atmospheric transparency window resulted in better behavior. Theoretical material M6, with an emissivity of 1, achieved the lowest heat gain of 3091 $Wh \cdot m^{-2}$.

If the average temperature increase in urban areas reaches the predicted 4 to 5 ºC, daytime radiative cooling materials are great candidates to counteract it. Radiative cooling is of special interest in cities suffering from the UHI effect since the heat accumulated during the day will be evacuated to outer space instead of to the streets, alleviating the heat buildup in cities and breaking the vicious cycle of increasing cooling demand. However, more research is necessary to determine how to apply this to the built environment. The impact of building radiation on the ability of these materials to cool down should be studied in more depth.

Table 3: Summary of simulations results.

Phoenix		**Sydney**	
Insulated			
Material	**ΔT (ºC) difference**	**Material**	**ΔT (ºC) difference**
M6	5,30 ºC	M7	4,21 ºC
RC2 Radicool	3,42 ºC	RC2 Radicool	2,36 ºC
RC1 Skycool	2,40 ºC	RC1 Skycool	1,55 ºC
CM5 White paint 2	3,12 ºC	CM5 White paint 2	2,04 ºC
CM4 White paint 1	2,52 ºC	CM4 White paint 1	1,41 ºC
Conductive			
Material	**Daily heat gains**	**Material**	**Daily heat gains**
M6	3091 $W \cdot m^{-2}$	M8	-3176 $W \cdot m^{-2}$
RC2 Radicool	4578 $W \cdot m^{-2}$	RC2 Radicool	-2213 $W \cdot m^{-2}$
RC1 Skycool	4644 $W \cdot m^{-2}$	RC1 Skycool	-1574 $W \cdot m^{-2}$
CM5 White paint 2	4897 $W \cdot m^{-2}$	CM5 White paint 2	-2077 $W \cdot m^{-2}$
CM4 White paint 1	5240 $W \cdot m^{-2}$	CM4 White paint 1	-1689 $W \cdot m^{-2}$

Declaration of interest

LC would like to acknowledge the funding of the Government of Navarre for an industrial Ph.D. research grant "Doctorados industriales 2018-2020” file number 0011-1408-2017-000028 at the University of the Basque Country that takes place in the R+D department of Alonso Hernández & asociados arquitectura S.L.

References

Aili, A., Zhao, D., Lu, J., Zhai, Y., Yin, X., Tan, G., Yang, R., 2019. A kW-scale, 24-hour continuously operational, radiative sky cooling system: Experimental demonstration and predictive modeling. Energy Conversion and Management 186, 586–596. https://doi.org/10.1016/j.enconman.2019.03.006

Algarni, S., Nutter, D., 2015. Survey of Sky Effective Temperature Models Applicable to Building Envelope Radiant Heat Transfer. ASHRAE Transactions 121, 351. https://doi.org/10.13140/rg.2.1.4212.5526

Anderson G. Brooke, Bell Michelle L., 2011. Heat Waves in the United States: Mortality Risk during Heat Waves and Effect Modification by Heat Wave Characteristics in 43 U.S. Communities. Environmental Health Perspectives 119, 210–218. https://doi.org/10.1289/ehp.1002313

Antonanzas-Torres, F., Urraca, R., Polo, J., Perpiñán-Lamigueiro, O., Escobar, R., 2019. Clear sky solar irradiance models: A review of seventy models. Renewable and Sustainable Energy Reviews 107, 374–387. https://doi.org/10.1016/j.rser.2019.02.032

Argiriou, A., Santamouris, M., Balaras, C., Jeter, S., 1992. Potential Of Radiative Cooling In Southern Europe. International Journal of Solar Energy 13, 189–203. https://doi.org/10.1080/01425919208909784

Aviv, D., Meggers, F., 2017. Cooling oculus for desert climate-dynamic structure for evaporative downdraft and night sky cooling, in: Energy Procedia. Presented at the CISBAT International Conference-Furture Buildings & Districts- Energy Efficiency from Nano to Urban Scale, CISBAT 2017, Lausanne, Switzerland, pp. 1124–1129. https://doi.org/10.1016/j.egypro.2017.07.474

Bartos, M., Chester, M., Johnson, N., Gorman, B., Eisenberg, D., Linkov, I., Bates, M., 2016. Impacts of rising air temperatures on electric transmission ampacity and peak electricity load in the United States. Environ. Res. Lett. 11, 114008. https://doi.org/10.1088/1748-9326/11/11/114008

Bell, J.M., Smith, G.B., Lehmann, R., 2003. Advanced Roof Coatings: Materials and their Applications, in: Conference Proceedings. Presented at the SASBE 2003 - Smart and Sustainable Built Environment, 19-21 November 2003, Brisbane, Australia.

Berdahl, P., Bretz, S.E., 1997. Preliminary survey of the solar reflectance of cool roofing materials. Energy and Buildings 25, 149–158. https://doi.org/10.1016/S0378-7788(96)01004-3

Berdahl, P., Fromberg, R., 1982. The Thermal Radiance of Clear Skies. Solar Energy 29, 299–314. https://doi.org/10.1016/0038-092X(82)90245-6

Berger, X., Bathiebo, J., 1989. From spectral clear sky emissivity to total clear sky emissivity. Solar & Wind Technology 6, 551–556. https://doi.org/10.1016/0741-983X(89)90090-8

Bliss, R.W., 1961. Atmospheric radiation near the surface of the ground: A summary for engineers. Solar Energy 5, 103–120. https://doi.org/10.1016/0038-092X(61)90053-6

Chen, Z., Zhu, L., Raman, A., Fan, S., 2016. Radiative cooling to deep sub-freezing temperatures through a 24-h day–night cycle. Nature Communications 7, 13729. https://doi.org/10.1038/ncomms13729

Cui, Y., Wang, Y., Huang, Q., Wei, S., 2016. Effect of radiation and convection heat transfer on cooling performance of radiative panel. Renewable Energy 99, 10–17. https://doi.org/10.1016/j.renene.2016.06.025

Eicker, U., Dalibard, A., 2011. Photovoltaic–thermal collectors for night radiative cooling of buildings. Solar Energy 85, 1322–1335. https://doi.org/10.1016/j.solener.2011.03.015

Energy – UN-Habitat, n.d. URL https://unhabitat.org/urban-themes/energy/ (accessed 11.4.19).

Erell, E., Etzion, Y., 1992. A Radiative Cooling System Using Water as a Heat Exchange Medium. Architectural Science Review 35, 39–49. https://doi.org/10.1080/00038628.1992.9696712

Erell, E., Yannas, S., Molina, J.L., 2006. Roof Cooling Techniques, in: The 23rd Conference on Passive and Low Energy Architecture. Presented at the PLEA2006, Geneva, Switzerland, pp. 175–191.

Feng, J., Gao, K., Santamouris, M., Shah, K.W., Ranzi, G., 2020. Dynamic impact of climate on the performance of daytime radiative cooling materials. Solar Energy Materials and Solar Cells 208, 110426. https://doi.org/10.1016/j.solmat.2020.110426

Foustalieraki, M., Assimakopoulos, M.N., Santamouris, M., Pangalou, H., 2017. Energy performance of a medium scale green roof system installed on a commercial building using numerical and experimental data recorded during the cold period of the year. Energy and Buildings 135, 33–38. https://doi.org/10.1016/j.enbuild.2016.10.056

Goldstein, E.A., Raman, A.P., Fan, S., 2017. Sub-ambient non-evaporative fluid cooling with the sky. Nature Energy 2, nenergy2017143. https://doi.org/10.1038/nenergy.2017.143

Herrera-Gomez, S.S., Quevedo-Nolasco, A., Pérez-Urrestarazu, L., 2017. The role of green roofs in climate change mitigation. A case study in Seville (Spain). Building and Environment 123, 575–584. https://doi.org/10.1016/j.buildenv.2017.07.036

Herrero, J, Polo, M.J., 2012. Hydrology and Earth System Sciences Parameterization of atmospheric longwave emissivity in a mountainous site for all sky conditions. Hydrol. Earth Syst. Sci 16, 3139–3147. https://doi.org/10.5194/hess-16-3139-2012

Herrero, J., Polo, M.J., 2012. Parameterization of atmospheric longwave emissivity in a mountainous site for all sky conditions. Hydrology and Earth System Sciences 16, 3139–3147. https://doi.org/10.5194/hess-16-3139-2012

Huang, Z., Ruan, X., 2017. Nanoparticle embedded double-layer coating for daytime radiative cooling. International Journal of Heat and Mass Transfer 104, 890–896. https://doi.org/10.1016/j.ijheatmasstransfer.2016.08.009

International Energy Agency, 2018. World Energy Outlook 2018. Executive Summary.

Kolokotroni, M., Gowreesunker, B.L., Giridharan, R., 2013. Cool roof technology in London: An experimental and modelling study. Energy and Buildings 67, 658–667. https://doi.org/10.1016/j.enbuild.2011.07.011

Kolokotsa, D.– D., Giannariakis, G., Gobakis, K., Giannarakis, G., Synnefa, A., Santamouris, M., 2018. Cool roofs and cool pavements application in Acharnes, Greece. Sustainable Cities and Society 37, 466–474. https://doi.org/10.1016/j.scs.2017.11.035

Kolokotsa, D., Santamouris, M., Zerefos, S.C., 2013. Green and cool roofs' urban heat island mitigation potential in European climates for office buildings under free floating conditions. Solar Energy 95, 118–130. https://doi.org/10.1016/j.solener.2013.06.001

Kottek, M., Grieser, J., Beck, C., Rudolf, B., Rubel, F., 2006. World Map of the Köppen-Geiger climate classification updated. Meteorologische Zeitschrift 259–263. https://doi.org/10.1127/0941-2948/2006/0130

Kou, J., Jurado, Z., Chen, Z., Fan, S., Minnich, A.J., 2017. Daytime Radiative Cooling Using Near-Black Infrared Emitters. ACS Photonics 4, 626–630. https://doi.org/10.1021/acsphotonics.6b00991

Lemonsu, A., Viguié, V., Daniel, M., Masson, V., 2015. Vulnerability to heat waves: Impact of urban expansion scenarios on urban heat island and heat stress in Paris (France). Urban Climate 14, 586–605. https://doi.org/10.1016/j.uclim.2015.10.007

Li, M., Peterson, H.B., Coimbra, C.F.M., 2019. Radiative cooling resource maps for the contiguous United States. Journal of Renewable and Sustainable Energy 11, 036501. https://doi.org/10.1063/1.5094510

Li, W., Shi, Y., Chen, K., Zhu, L., Fan, S., 2017. A Comprehensive Photonic Approach for Solar Cell Cooling. ACS Photonics 4, 774–782. https://doi.org/10.1021/acsphotonics.7b00089

Malek, E., 1997. Evaluation of effective atmospheric emissivity and parameterization of cloud at local scale. Atmospheric Research 45, 41–54. https://doi.org/10.1016/S0169-8095(97)00020-3

Martin, M., Berdahl, P., 1984. Characteristics of infrared sky radiation in the United States. Solar Energy 33, 321–336. https://doi.org/10.1016/0038-092X(84)90162-2

Meteonorm 7, 2017. . Meteotest, Bern, Switzerland.

Miller, W., Crompton, G., Bell, J., 2015. Analysis of Cool Roof Coatings for Residential Demand Side Management in Tropical Australia. Energies 8, 5303–5318. https://doi.org/10.3390/en8065303

Monteith, J.L., Unsworth, M.H., 2013. Principles of Environmental Physics. Plants, Animals, and the Atmosphere, Fourth. ed. Elsevier.

Oke, T.R., Johnson, G.T., Steyn, D.G., Watson, I.D., 1991. Simulation of surface urban heat islands under 'ideal' conditions at night part 2: Diagnosis of causation. Boundary-Layer Meteorol 56, 339–358. https://doi.org/10.1007/BF00119211

O'Neill, B.C., Liddle, B., Jiang, L., Smith, K.R., Pachauri, S., Dalton, M., Fuchs, R., 2012. Demographic change and carbon dioxide emissions. The Lancet 380, 157–164. https://doi.org/10.1016/S0140-6736(12)60958-1

Radhi, H., Sharples, S., Taleb, H., Fahmy, M., 2017. Will cool roofs improve the thermal performance of our built environment? A study assessing roof systems in Bahrain. Energy and Buildings 135, 324–337. https://doi.org/10.1016/j.enbuild.2016.11.048

Raman, A.P., Anoma, M.A., Zhu, L., Rephaeli, E., Fan, S., 2014. Passive radiative cooling below ambient air temperature under direct sunlight. Nature 515, 540–544. https://doi.org/10.1038/nature13883

Rephaeli, E., Raman, A., Fan, S., 2013. Ultrabroadband Photonic Structures To Achieve High-Performance Daytime Radiative Cooling. Nano Letters 13, 130311121615001. https://doi.org/10.1021/nl4004283

Santamouris, M., 2020. Recent progress on urban overheating and heat island research. Integrated assessment of the energy, environmental, vulnerability and health impact. Synergies with the global climate change. Energy and Buildings 207, 109482. https://doi.org/10.1016/j.enbuild.2019.109482

Santamouris, M., 2019. Minimizing Energy Consumption, Energy Poverty and Global and Local Climate Change in the Built Environment: Innovating to Zero. Elsevier. https://doi.org/10.1016/C2016-0-01024-0

Santamouris, M., 2013. Using cool pavements as a mitigation strategy to fight urban heat island—A review of the actual developments. Renewable and Sustainable Energy Reviews 26, 224–240. https://doi.org/10.1016/j.rser.2013.05.047

Santamouris, M., Feng, J., 2018. Recent Progress in Daytime Radiative Cooling: Is It the Air Conditioner of the Future? Buildings 8, 168. https://doi.org/10.3390/buildings8120168

Santamouris, M., Haddad, S., Saliari, M., Vasilakopoulou, K., Synnefa, A., Paolini, R., Ulpiani, G., Garshasbi, S., Fiorito, F., 2018. On the energy impact of urban heat island in Sydney: Climate and energy potential of mitigation technologies. Energy and Buildings 166, 154–164. https://doi.org/10.1016/j.enbuild.2018.02.007

Santamouris, M., Kolokotsa, D., 2015. On the impact of urban overheating and extreme climatic conditions on housing, energy, comfort and environmental quality of vulnerable population in Europe. Energy and Buildings, Renewable Energy Sources and Healthy Buildings 98, 125–133. https://doi.org/10.1016/j.enbuild.2014.08.050

Santamouris, M., Papanikolaou, N., Livada, I., Koronakis, I., Georgakis, C., Argiriou, A., Assimakopoulos, D.N., 2001. On the impact of urban climate on the energy consumption of buildings. Solar Energy, Urban Environment 70, 201–216. https://doi.org/10.1016/S0038-092X(00)00095-5

Santamouris, M., Synnefa, A., Kolokotsa, D., Dimitriou, V., Apostolakis, K., 2008. Passive cooling of the built environment - use of innovative reflective materials to fight heat islands and decrease cooling needs. International Journal of Low-Carbon Technologies 3, 71–82. https://doi.org/10.1093/ijlct/3.2.71

Shi, Y., Li, W., Raman, A., Fan, S., 2018. Optimization of Multilayer Optical Films with a Memetic Algorithm and Mixed Integer Programming. ACS Photonics 5, 684–691. https://doi.org/10.1021/acsphotonics.7b01136

Smith, G.B., 2009. Amplified radiative cooling via optimised combinations of aperture geometry and spectral emittance profiles of surfaces and the atmosphere. Solar Energy Materials and Solar Cells 93, 1696–1701. https://doi.org/10.1016/j.solmat.2009.05.015

Sugita, M., Brutsaert, W., 1993. Cloud effect in the estimation of instantaneous downward longwave radiation. Water Resources Research 29, 599–605. https://doi.org/10.1029/92WR02352

Vall, S., Castell, A., 2017. Radiative cooling as low-grade energy source: A literature review. Renewable and Sustainable Energy Reviews 77, 803–820. https://doi.org/10.1016/j.rser.2017.04.010

Vall, S., Castell, A., Medrano, M., 2018. Energy Savings Potential of a Novel Radiative Cooling and Solar Thermal Collection Concept in Buildings for Various World Climates. Energy Technology 6, 2200–2209. https://doi.org/10.1002/ente.201800164

Wang, W., Fernandez, N., Katipamula, S., Alvine, K., 2018. Performance assessment of a photonic radiative cooling system for office buildings. Renewable Energy 118, 265–277. https://doi.org/10.1016/j.renene.2017.10.062

World Urbanization Prospects (No. ST/ESA/SER.A/366), 2014. . United Nations, Department of Economic and Social Affairs.

Yellot, J.I., 1976. Early Tests of the “Skytherm” System. Presented at the Passive solar heating and cooling conference and workshop proceedings, Merily H. Keller, LASL, University of New Mexico, Albuquerque, New Mexico, pp. 54–62.

Yellot, John I., S., 1976. Solar Roof Ponds, “Early Tests of the ‘Skytherm’ System.” Presented at the Passive solar heating and cooling conference and workshop proceedings, Merily H. Keller, LASL, University of New Mexico, Albuquerque, New Mexico, pp. 54–62.

Zhai, Y., Ma, Y., David, S.N., Zhao, D., Lou, R., Tan, G., Yang, R., Yin, X., 2017. Scalable-manufactured randomized glass-polymer hybrid metamaterial for daytime radiative cooling. Science 355, 1062–1066. https://doi.org/10.1126/science.aai7899

Zhang, K., Zhao, D., Yin, X., Yang, R., Tan, G., 2018. Energy saving and economic analysis of a new hybrid radiative cooling system for single-family houses in the USA. Applied Energy 224, 371–381. https://doi.org/10.1016/j.apenergy.2018.04.115

Zhao, D., Aili, A., Yin, X., Tan, G., Yang, R., 2019. Roof-integrated radiative air-cooling system to achieve cooler attic for building energy saving. Energy and Buildings 203, 109453. https://doi.org/10.1016/j.enbuild.2019.109453

Zhou, L., Song, H., Liang, J., Singer, M., Zhou, M., Stegenburgs, E., Zhang, N., Ng, T.K., Yu, Z., Ooi, B., Gan, Q., 2019a. All-day radiative cooling using beam-controlled architectures, in: Conference on Lasers and Electro-Optics (2019), Paper ATh1I.2. Presented at the CLEO: Applications and Technology, Optical Society of America, p. ATh1I.2. https://doi.org/10.1364/CLEO_AT.2019.ATh1I.2

Zhou, L., Song, H., Liang, J., Singer, M., Zhou, M., Stegenburgs, E., Zhang, N., Xu, C., Ng, T., Yu, Z., Ooi, B., Gan, Q., 2019b. A polydimethylsiloxane-coated metal structure for all-day radiative cooling. Nat Sustain 2, 718–724. https://doi.org/10.1038/s41893-019-0348-5

Zhu, L., Fiorino, A., Thompson, D., Mittapally, R., Meyhofer, E., Reddy, P., 2019. Near-field photonic cooling through control of the chemical potential of photons. Nature 566, 239–244. https://doi.org/10.1038/s41586-019-0918-8

Zhu, L., Raman, A.P., Fan, S., 2015. Radiative cooling of solar absorbers using a visibly transparent photonic crystal thermal blackbody. Proceedings of the National Academy of Sciences 112, 12282–12287. https://doi.org/10.1073/pnas.1509453112

Zinzi, M., Agnoli, S., 2012. Cool and green roofs. An energy and comfort comparison between passive cooling and mitigation urban heat island techniques for residential buildings in the Mediterranean region. Energy and Buildings 55, 66–76. https://doi.org/10.1016/j.enbuild.2011.09.024